THE JOURNAL OF PHYSICAL CHEMISTRY C

Article

pubs.acs.org/JPCC

Direct and Reverse Chemical Garden Patterns Grown upon Injection in Confined Geometries

Florence Haudin,[†] Julyan H. E. Cartwright,[‡] and A. De Wit*[,†]

[†]Nonlinear Physical Chemistry Unit, Faculté des Sciences, Université libre de Bruxelles (ULB), CP231, 1050 Brussels, Belgium

[‡]Instituto Andaluz de Ciencias de la Tierra, CSIC-Universidad de Granada, Campus Fuentenueva, E-18071 Granada, Spain

ABSTRACT: Spatial precipitate patterns resulting from the growth of chemical gardens in a confined quasi-two-dimensional horizontal geometry are studied experimentally upon radial injection of a solution of one reactant into the other at a fixed flow rate. We show that, at large enough concentrations, the patterns are different when injecting a solution of cobalt chloride into a solution of silicate (the direct case) than in the reverse case of silicate displacing the metal-ion solution. We discuss the possible influences of the viscosity ratio, density difference, pH, and concentrations of the reactants on the dynamics observed and characterize quantitatively the growth of some typical structures.

I. INTRODUCTION

Whether one given fluid is injected into another one or the reverse can lead to quite different types of flows if the fluids have different properties. As an example, the interface between the fluids is unstable with regard to viscous fingering if a less viscous fluid displaces a more viscous one, while it remains stable in the reverse case.[1,2] Similarly, a dissolution front leading to an increase in permeability (and hence in mobility) behind it can lead to channeling, while a precipitation front is stable.[3,4]

Recently, chemical reactions have been shown also to induce asymmetries in the patterns obtained by injection of one reactive solution into another and even to be able to destabilize displacement cases that would be stable in nonreactive conditions.[5−10] For instance, Podgorski et al. have shown experimentally that fingering can be obtained in the reaction zone between aqueous solutions of different solutes A and B upon formation of a gel by reaction between A and B.[5] The patterns are different whether A is injected into B or vice versa even though the viscosities of the reactant solutions are the same. Similarly, local precipitation in the reactive zone between two aqueous solutions of different reactants A and B can induce fingering,[10] the properties of which are different depending on whether A is the injected or displaced solution. Numerical simulations of related problems show that direct or reverse injection does not produce the same pattern and that the underlying properties of the A + B → C reaction−diffusion (RD) fronts may have an effect on this asymmetry.[7,9,10]

Such results suggest that reaction−diffusion−convection (RDC) patterns obtained upon injection of one chemical into the other with changes in either viscosity or permeability due to a reaction can be different depending on whether A is injected into B or the reverse. This asymmetry could be applied to select the type of pattern formed and the related product generated, by selectively controlling which reactant is injected into which. We develop this idea here by analyzing the differences between direct and reverse chemical gardens grown upon injection of a metal salt solution into silicate or vice versa in confined two-dimensional geometries.

Chemical gardens, when grown in a beaker, produce plantlike mineral structures first described in the 17th century[11] and popularly known from chemistry sets for children. They are classically grown in three-dimensional (3D) containers by placing a solid metal salt seed into a silicate solution. When the metal salt starts dissolving in the silicate solution, a semipermeable membrane forms by precipitation across which water is pumped by osmosis from the silicate solution into the metal salt solution, further dissolving the salt. Silicate is most often employed, but many other anions such as carbonate or oxalate can also be used. Above a given pressure, the membrane breaks. The dissolved metal salt solution, being generally less dense than the reservoir silicate solution, rises as a buoyant jet through the broken membrane and further precipitates in contact with the silicate solution, producing a collection of mineral forms that resemble a garden. This 3D growth results from a complex combination of osmosis, buoyancy, and reaction−diffusion processes.[12−15]

Chemical gardens also are interesting for the formation of chemical motors[16] and pressure oscillators,[17,18] for building microfluidic-type devices[19] that can be produced by optical control[20] or by bubble guidance,[21] for energy storage purposes,[22] as catalytic and self-assembled layered materials.[23−27] Chemical gardens moreover reproduce conditions similar to those present

Received: January 26, 2015
Revised: May 16, 2015
Published: June 25, 2015

DOI: 10.1021/acs.jpcc.5b00599
J. Phys. Chem. C 2015, 119, 15067−15076

at hydrothermal vents in the primitive ocean where the first forms of life may have appeared.[28,29] To gain more control over the reproducibility of the precipitate tubes, chemical gardens have also been studied in 3D by injecting directly solutions of metallic salt into sodium silicate solutions:[30] different regimes called jetting, popping, or budding have been reported depending on the concentrations of the reactants and on the flow rate. Reverse chemical gardens have also been studied with a single silicate particle glued to a glass rod, as a seed put at the surface of a metallic salt solution.[31] They show the same dynamical regimes of jetting, popping, or budding and the existence of an additional one called fracturing.

Recently, experiments in quasi-2D systems have been performed by injection of one solution of a metallic salt into a solution of silicate (the so-called "direct chemical garden").[32,33] Confinement in the thin gap of a horizontal cell[10] decreases the effect of buoyancy, whereas the use of injection limits the osmotic effects. Different patterns, generic with regard to changes in the chemicals,[33] have been observed when the concentrations are changed. In parallel, it has been demonstrated, using another precipitating reaction with injection in thin solution layers, that injection can stabilize thermodynamically unstable species compared to what happens in a stirred batch reactor.[34] This raises the question of the importance of the flow conditions on the selection of the precipitate and on its macroscopic self-organization.

In this context, our objective is here to analyze in confined chemical gardens to what extent the choice of the injected and displaced solutions influences the patterns obtained and how their shape varies with the relative concentration and physical properties of the solutions. To do so, we study the differences between precipitates of reverse or direct gardens grown by injecting silicate into the metallic salt solution or vice versa in a confined geometry. We analyze the influence of the change in viscosity ratio, density difference, pH, and concentrations of the reactants in various regimes to try to understand which factors are important in the pattern selection.

The article is organized as follows. We first describe in section II the experimental setup and show the various patterns obtained in both direct and reverse gardens grown upon injection in a confined geometry at a fixed injection flow rate. We next discuss in section III the changes in various parameters of the problem in the different regimes. A quantitative comparison between some of the patterns is performed in section IV before conclusions are drawn in section V.

II. DIRECT AND REVERSE CONFINED PRECIPITATION PATTERNS

The confinement is obtained in a horizontal Hele-Shaw cell, consisting of two transparent acrylate plates separated by a gap of 0.5 mm. The cell initially filled by a solution of one reactant is placed on top of a light table providing a diffuse light. The solution of the other reactant is injected radially from the center at a fixed flow rate Q using a syringe pump. The dynamics is recorded from above using a complementary metal oxide semiconductor (CMOS) camera. As reactants, we use a sodium silicate solution of concentration C_{Si} prepared by dilution of a commercial solution of concentration 6.25 M with respect to silica SiO_2 (Sigma-Aldrich) and a cobalt chloride solution of concentration C_{Co}, prepared by dissolution in water of a hydrated $CoCl_2{\cdot}6H_2O$ salt (Sigma-Aldrich). The properties of the different solutions are reported in Tables 1 and 2. The morphologies of the pattern can vary when the flow rate is changed, but this effect will not be addressed here, as we keep the flow rate Q constant and equal to 0.11 mL/s for all our experiments.

Table 1. Density, pH and viscosity of the cobalt chloride solutions. The measurements are performed at room temperature

C_{Co} (M)	0.10	0.25	0.63	1.00	1.38
ρ (g.cm^{-3})	1.01	1.03	1.07	1.11	1.15
pH	5.4	4.6	4.1	3.7	3.4
μ (mPa.s)	1.1	1.2	1.4	1.6	1.7

Table 2. Density, pH and viscosity of the sodium silicate solutions. The measurements are performed at room temperature

C_{Si} (M)	0.25	0.63	1.25	3.13	6.25
ρ (g.cm^{-3})	1.02	1.04	1.09	1.21	1.42
pH	11.6	11.6	11.7	11.7	11.8
μ (mPa.s)	1.2	1.3	1.7	3.6	≈40

We recall first the various dynamics observed in the case of direct chemical gardens, i.e., when the cobalt solution is injected into the silicate one (Figure 1). The experimental snapshots correspond to the same experiments as in Haudin et al.[32] but are shown here after 30 s in order to better appreciate the effects of leakage from the precipitate layers that appear at larger times. Depending on the relative concentrations of reactants, patterns such as flowers, filaments, worms, hairs, lobes, and spirals are obtained. The type of pattern obtained is generic for given values of concentrations. Similar patterns have been observed for different reactants as well.[33] The number and orientation of filaments, spirals, or flower petals vary however from one experiment to the other. The spirals have been proven to be logarithmic and understood in terms of a minimal geometrical model based on the rupture of a solid precipitate growing initially as a circle.[32]

The direct patterns can be compared to those obtained in reverse chemical gardens (Figure 2). When both concentrations are small (in the lower left corner of the phase diagrams), the patterns are similar whether the sodium silicate is the displaced or the injected solution. In both reverse and direct cases, a thin dark precipitate appears in the contact zone between the two reactants, deforming into various shapes like protuberances (lobes) or coiling into arcs of spirals. For the lobes in the reverse case, secondary structures similar to the fan structures reported by Podgorski et al. (see Figures 1 and 3d in ref 5) are forming at the periphery of the first pattern. The spirals are still observed in a large part of the parameter space.

Differences between direct and reverse structures appear when one of the two concentrations, or both of them, are larger. At C_{Si} = 0.25 M, the patterns appear different for C_{Co} = 0.63 M or larger. In the direct case, the patterns are made of hairs because of a destabilization of the initially circular invading cobalt chloride solution, while lobes are observed in the reverse case, with secondary filamentous structures growing between the lobes. For C_{Si} = 0.63 M and larger C_{Co}, the initial direct patterns are worms, with terrace-like secondary structures growing tangentially to the first material. In the reverse case, the patterns are quite large spirals. The number of spirals around the injection point is not fixed and depends on the initial number of breaks in the precipitate. For C_{Co} = 1 or 1.38 M, dark connecting structures looking like tubes grow in some cases between the spirals.

DOI: 10.1021/acs.jpcc.5b00599
J. Phys. Chem. C 2015, 119, 15067−15076

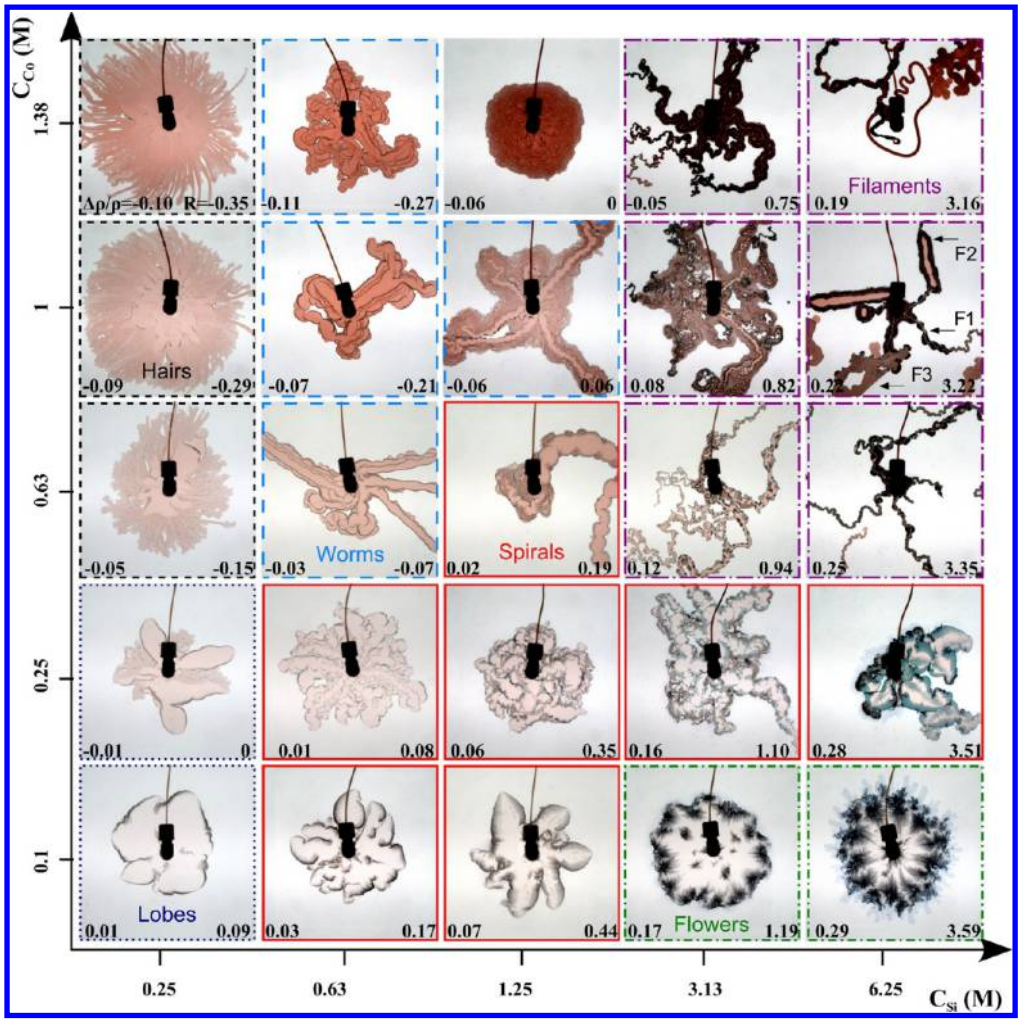

Figure 1. Classification of direct confined chemical gardens in a parameter space spanned by the concentration C_{Co} of the injected aqueous solution of cobalt chloride and the concentration C_{Si} of the displaced aqueous solution of sodium silicate. The diagram is divided into different colored frames referring to the various classes of patterns observed: lobes (dotted dark blue), spirals (solid red), hairs (dashed black), flowers (dashed-dotted green), filaments (long dashed-dotted purple), and worms (long dashed blue). The field of view is 15 cm × 15 cm, shown 30 s after injection starts. The number on the lower right corner is the log mobility ratio R, while the one on the left expresses the normalized difference of density $\Delta\rho/\rho = (\rho_{Si} - \rho_{Co})/\rho_{Si}$.

The direct compact circular pink solid phase observed in the direct case at C_{Co} = 1.38 M and C_{Si} = 1.25 M is quite different from the reverse pattern made of a succession of spirals growing in channels. Eventually, when both reactants are concentrated, small filaments F1 are observed in the direct case[32,33] while large shells with a smooth rim dominate in the reverse one, as also shown in Figure 3a. We notice nevertheless that sometimes, between large shells, there are smaller connecting structures that are similar to the filaments, suggesting that both structures can coexist in the same range of concentrations in the reverse case. Note also that for filaments F1 in the direct case, there are transitions to other structures, filaments F2 quite similar to worms but with thicker walls, or shells at smaller scale called filaments F3, with some experiments presenting a mixture of several of them,[33] as shown with arrows on Figure 1. A zoom-in on a shell structure observed in the direct case as a possible structure other than the filaments is shown in Figure 3b for cobalt sulfate as the injected fluid. As it is generally the case in chemical gardens,[33,36] the patterns have been shown to be independent of the counterion Cl^- or SO_4^{2-}.

III. PHYSICAL AND CHEMICAL PARAMETERS

Physical and chemical parameters that may influence the pattern selection are the viscosity, the density, the pH, and the concentrations of both reactant solutions and the mechanical properties of the precipitates formed. The flow rate is a further important parameter of the problem, but in this study, it was kept constant. Chemical and mechanical characterizations of the solid phases formed are also beyond the scope of the present paper. We report here the differences between reverse and direct patterns and discuss the possible influence of the different parameters mentioned above in the pattern selection.

A. Viscosity Contrast. To understand the possible role of the viscosity ratio between the two solutions, the log mobility ratio $R = \log(\mu_{Si}/\mu_{Co})$ between the two reactants has been computed and is reported in each panel of Figure 1. If $R > 0$, then in the direct case the displaced silicate solution is more viscous and a viscous fingering instability may take place. Then the larger R, the more intense is the fingering. On the contrary, if $R < 0$, the direct displacement is viscously stable, unless another source of instability arises because of the precipitation or of buoyancy effects. The reverse trend (i.e., stability for $R > 0$ and viscous

DOI: 10.1021/acs.jpcc.5b00599
J. Phys. Chem. C 2015, 119, 15067−15076

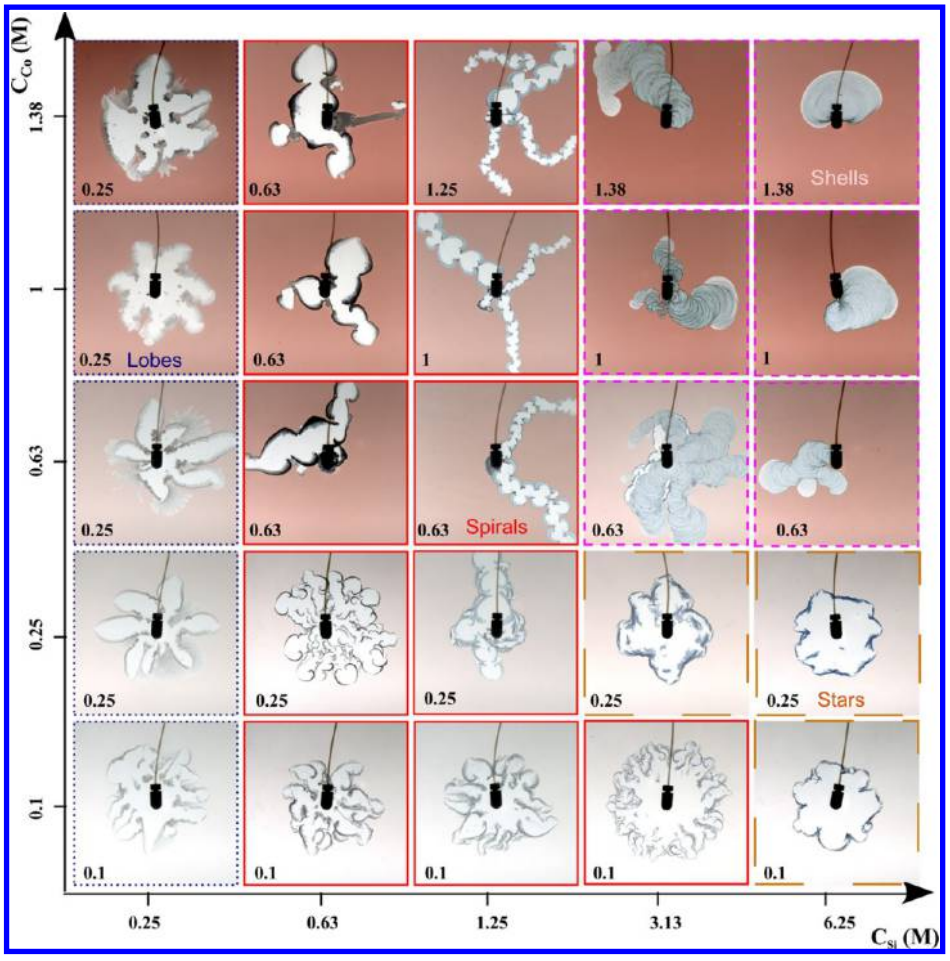

Figure 2. Classification of reverse confined chemical gardens in a parameter space spanned by the concentration C_{Si} of the injected aqueous solution of sodium silicate and the concentration C_{Co} of the displaced aqueous solution of cobalt chloride. The diagram is divided into different colored frames referring to the various classes of patterns observed: lobes (dotted dark blue), spirals (solid red), stars (large dashed-gold), and shells (dashed-pink). As in Figure 1, the field of view is 15 cm × 15 cm, shown 30 s after injection starts. The number on the left lower corner gives the value of C_I (M), the smallest concentration of both reactants.

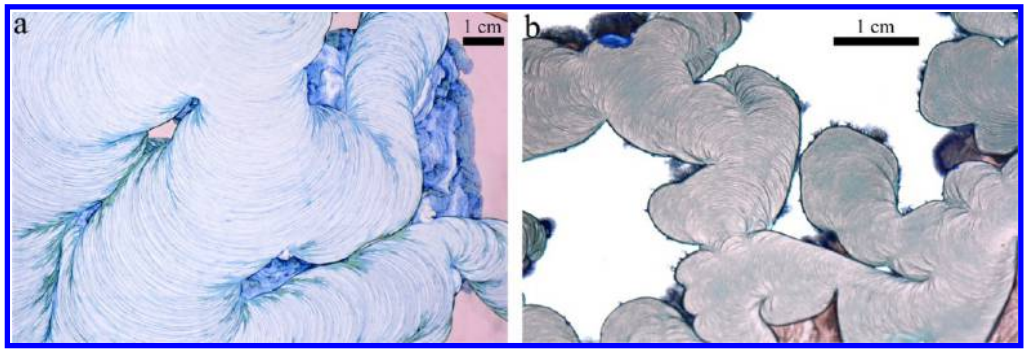

Figure 3. Zoom on shell structures in (a) the reverse case with $CoCl_2$ and (b) the direct case with $CoSO_4$ as the injected reactant. The pictures are taken a few minutes after the end of the injection.

fingering if $R < 0$) holds for the reverse garden when the silicate solution is injected into the cobalt chloride one.

To evaluate the effect of the viscosity ratio in the difference between direct and reverse patterns, we have performed two nonprecipitating tests consisting of injecting dyed water into the silicate solutions. For our given fixed flow rate and size of the Hele-Shaw cell, viscous fingering is observed only at the largest concentration C_{Si} = 6.25 M of silicate ($R_w = \log(\mu_{Si}/\mu_{water})$ = 3.7 as in the fifth column of Figures 1 and 2). For C_{Si} = 3.13 M (R_w = 1.3) and below this value, the nonprecipitating miscible interface remains stable, which shows that the viscosity ratio is sufficiently large to trigger viscous fingering only in the fifth column of Figure 1, while it is not a key ingredient in the pattern selection for the first four columns of Figure 1 and in the reverse case of Figure 2.

Note that in the fifth column of Figure 1, even if the viscosity ratio is high enough to trigger a viscous instability in the nonprecipitating case, the reactive patterns vary depending on the concentration of the injected cobalt chloride solution C_{Co}.

DOI: 10.1021/acs.jpcc.5b00599
J. Phys. Chem. C 2015, 119, 15067−15076

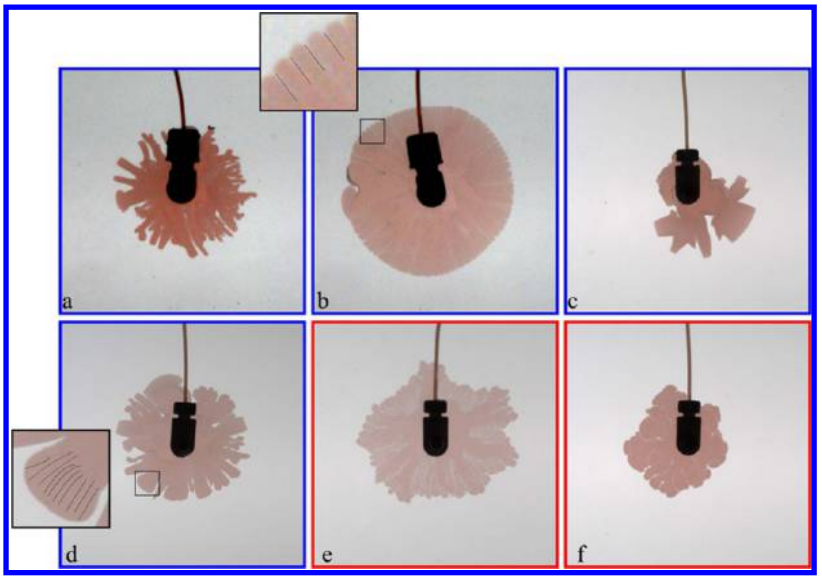

Figure 4. Direct chemical garden patterns at t = 7.5 s (a–d) four different patterns obtained for the same set of concentrations, C_{Co} = 1.38 M injected into C_{Si} = 0.25 M ($\Delta\rho/\rho = -0.10$, blue frames); (e, f) same concentrations C_{Co} and C_{Si} but the density of the silicate solution is equal to that of the cobalt chloride by addition of sucrose ($\Delta\rho/\rho \approx 0$, red frames). In the black-framed squares with features zoomed 4 times, we highlight a few wavelengths of either the hairs (b) or of the underlying buoyancy stripes (d). The field of view is 10 cm × 10 cm.

For the lowest concentration C_{Co} = 0.1 M, the precipitate is not very cohesive and is therefore shaped in the direct case by the underlying viscous fingering instability to give flowers with a large amount of precipitate because of an increase in convective mixing. On the contrary, in the viscously stable displacement of the reverse case, we observe stars and less precipitate.

If strongly cohesive precipitate layers are formed, as happens above C_{Co} = 0.25 M, spirals or filaments are formed in the direct case while shells emerge in the reverse one. The viscously stabilizing effects may account for the more regular shape of the shells; however, the fact that we have spirals in both the direct and the reverse cases indicates that the viscosity ratio is not a key ingredient for the selection of these structures. While the mechanism of formation of filaments is still unclear, it has been shown previously that the growth mechanism of spirals is related to a self-similar growth of a solid membrane breaking at some point under the pressure of injection.[32]

These various considerations lead us to conclude that viscous effects are mainly important in understanding the difference between direct flowers influenced by a viscous fingering instability and reverse stars developing in a viscously stable flow but not in the formation of other patterns.

B. Density Contrast. In Figure 1, in addition to the log mobility ratio, we also display the normalized density contrast $\Delta\rho/\rho = (\rho_{Si} - \rho_{Co})/\rho_{Si}$ between the two reactant solutions in order to understand the possible role of the density difference between the two solutions. If $\Delta\rho/\rho \neq 0$, even if the system is quasi-bidimensional, destabilization due to density difference may occur, leading to the formation of buoyancy-driven stripes observed in nonreactive displacements.[37] Such buoyancy effects have also been observed in precipitation by injection in thin solution layers where the precipitate appears along the streamlines of the convective currents[38] and has a composition that can be different from that in homogeneous stirring conditions.[34] In the present reactive experiments, buoyancy-driven stripes may be observed when one reactant is in excess compared to the other one, which is when the amount and the mechanical strength of the precipitate are small.

This is typically the situation corresponding to the patterns referred to as hairs. Thus, to determine whether buoyancy effects are important in the shaping of hairs in the direct case, we compare in Figure 4 four different runs of experiments with hairs for C_{Co} = 1.38 M injected in C_{Si} = 0.25 M ($\Delta\rho/\rho = -0.10$) with two experiments in which a large amount of sucrose (around 36% in weight) has been added to the silicate in order to obtain an equidensity situation ($\Delta\rho/\rho \approx 0$). Note that the addition of sucrose increases the viscosity of the outside silicate solution to about 4 mPa·s, but as previously explained, such a viscosity jump should not be determinant in the pattern selection. We can see that for the hairs, the system is quite sensitive to the initial condition, as the four different runs with a density jump show quite compact hairs in a circular shape (Figure 4b), an internal circle destabilized in some hairs (Figure 4a and d), or more complex turnovers (Figure 4c). The patterns of the equidensity experiments (Figure 4e and Figure 4f) look different, with channels with less precipitate between more compact ones, similar to some of the patterns obtained by Podgorski et al. in a gel-producing reaction (see Figure 2d of ref 5). Nevertheless, the average characteristic size of the hairs (Figure 4b) is larger than the wavelength of the buoyancy stripes shown in Figure 4d. Hence, while we can conclude that the difference in density must play a role in the dynamics of hairs, as they are different from the patterns obtained when equalizing the two densities using sucrose, the size of the hairs is different from the characteristic wavelength of the buoyancy stripes.

C. Concentration of the Reactants. It is also instructive to compute $C_l = \min(C_{Si}, C_{Co})$, i.e., the smallest concentration from that of both reactants, which gives an idea of how much product can be produced. The larger C_l, the larger is the amount of precipitate formed in the reaction zone at fixed injection conditions. The values of C_l are given in Figure 2 but are equal for each panel of Figure 1 at the same concentrations.

For the lobes that exist in both direct and reverse cases (lower left of Figures 1 and 2), both R and $\Delta\rho/\rho$ are nearly zero, which suggests that viscosity or density difference effects are negligible

DOI: 10.1021/acs.jpcc.5b00599
J. Phys. Chem. C 2015, 119, 15067–15076

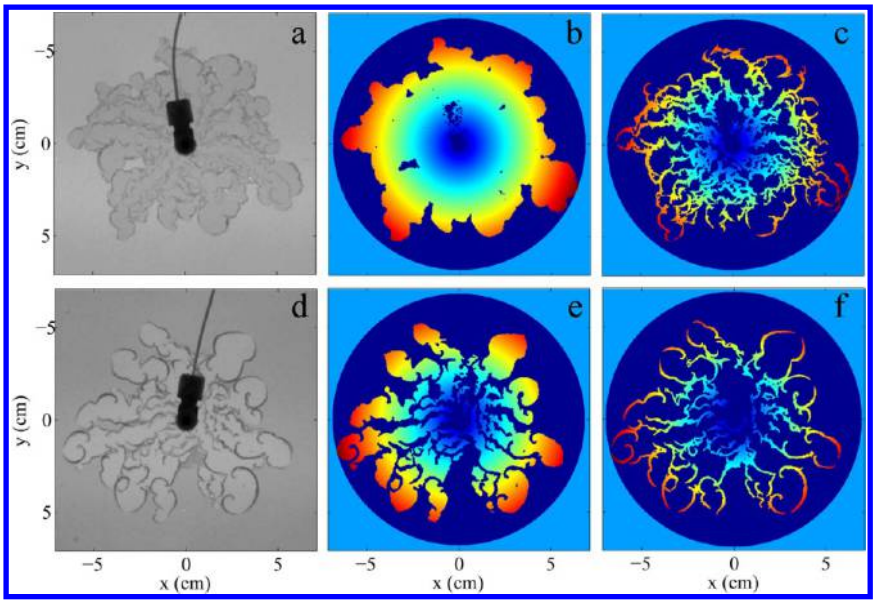

Figure 5. First line: direct case and second line: reverse case for C_{Co} = 0.25 M and C_{Si} = 0.63 M: (a, d) blue channel of the experimental snapshots, 30 s after the beginning of the injection; (b, c, e, f) $I \times r$ in false colors for different thresholds (b) 0.97, (c) 0.905, (e) 0.98, and (f) 0.94, capturing different features of the patterns, with I the digitized picture and r the radial distance from the injection point. The larger the threshold, the larger is the captured area. The dark blue disk enables us to visualize R_{max}. The field of view is 14.2 cm × 14.2 cm.

in both cases. The value of C_l in that case is rather small, and the thin precipitate layer is advected by the flow.

In the spiral domains, if one follows the third column of the reverse diagram from bottom to top (fixed C_{Si} = 1.25 M and increasing cobalt chloride concentrations), all the patterns are composed of spiraling precipitates but their distribution in space is different. For the smallest concentrations, the distribution is quite radial, whereas for the larger one, the structures are channels of spirals. Increasing C_l along this column thus seems to lead to transitions from radial to more directional growth. This could be related to an increased cohesivity of the more concentrated precipitate when C_l increases. In the fifth column, we note that viscous effects are not the key factor when $C_l > 0.25$, yet again the look of the pattern changes when C_l increases, which points to the usefulness of this parameter to try to understand whether the precipitate is cohesive enough to resist hydrodynamic instabilities.

D. Role of pH. In chemical-garden experiments, a steep pH gradient exists between the two reactant solutions. To determine the possible role of the pH, we have measured it for the 10 solutions used, as reported in Tables 1 and 2. We can see that in the direct case, the injected solution is encountering a silicate solution that has a pH close to 12, whereas in the reverse case, the alkaline injected solution is put in contact with an acidic one with pH between 3 and 5. It has been checked in the direct case that the patterns are not influenced by a decrease in pH of the metallic salt solution.[33] Furthermore, two tests have been performed with 6.25 M silicate solution injected into sulfuric acid. At pH ≈ 3, there is no precipitation of the silicate. This occurs at lower pH ≈ 1. This suggests that the pH of the injected solution is not influencing the pattern selection here but that it is rather the concentration values that are determinant.

E. Mechanical Resistance to the Flow. Precipitation coupled to the flow can lead to different materials in the reverse and in the direct case. We can suppose that, as for 3D tubes,[35,36] the precipitates produced are formed of different layers, with one material on the inner side and another material on the outer side of the semipermeable membranes formed. These membranes can hence have a different mechanical resistance to the flow, to fracture, and to leakage depending on which are the injected and displaced reactants.

For instance, if one looks at the direct and reverse patterns observed for C_{Co} = 1.38 M and C_{Si} = 1.25 M, as R and $\Delta\rho/\rho$ are very small for these concentrations, it is unlikely that density or viscosity difference effects are at play in both cases. The difference between them is then probably related to different mechanical properties of the precipitate depending whether silicate is the injected or displaced solution. Further investigations are needed to characterize the mechanical properties of the precipitates.

IV. DATA ANALYSIS

We can also quantitatively illustrate the differences of growth in the direct and the reverse cases by processing some of the experimental pictures, for instance, with spirals for C_{Co} = 0.25 M and C_{Si} = 0.63 M (Figures 5 and 6). The data processing consists of detecting the spatial domain spanned by the injected fluid and the precipitate after binarizing the pictures according to a given suitable threshold. In Figure 6, we compute during the first 30 s of the injection process, the temporal evolution of (i) the area $\mathcal{A}$ of the injected fluid, of the solid membrane, and of their sum, (ii) R_{max}, the radius of the circle encompassing the furthest point of the pattern from the injection point, and (iii) the density of the pattern defined[39] as $\mathcal{A}/(\pi R_{max}^2)$. We can in this way study the changes in time of the spatial distribution of both the injected fluid and of the precipitate layers. In Figure 5a and Figure 5d, we show the blue channel of the RGB experimental pictures, which is the one with the largest contrast for pictures involving a pink reactant like cobalt chloride. In Figure 5c−f are displayed in false colors the product $I \times r$ with I the digitized intensity and r the radial distance from the center. The disk of radius R_{max} is shown in dark blue. The spirals in the reverse case have apparently thicker walls.

DOI: 10.1021/acs.jpcc.5b00599
J. Phys. Chem. C 2015, 119, 15067−15076

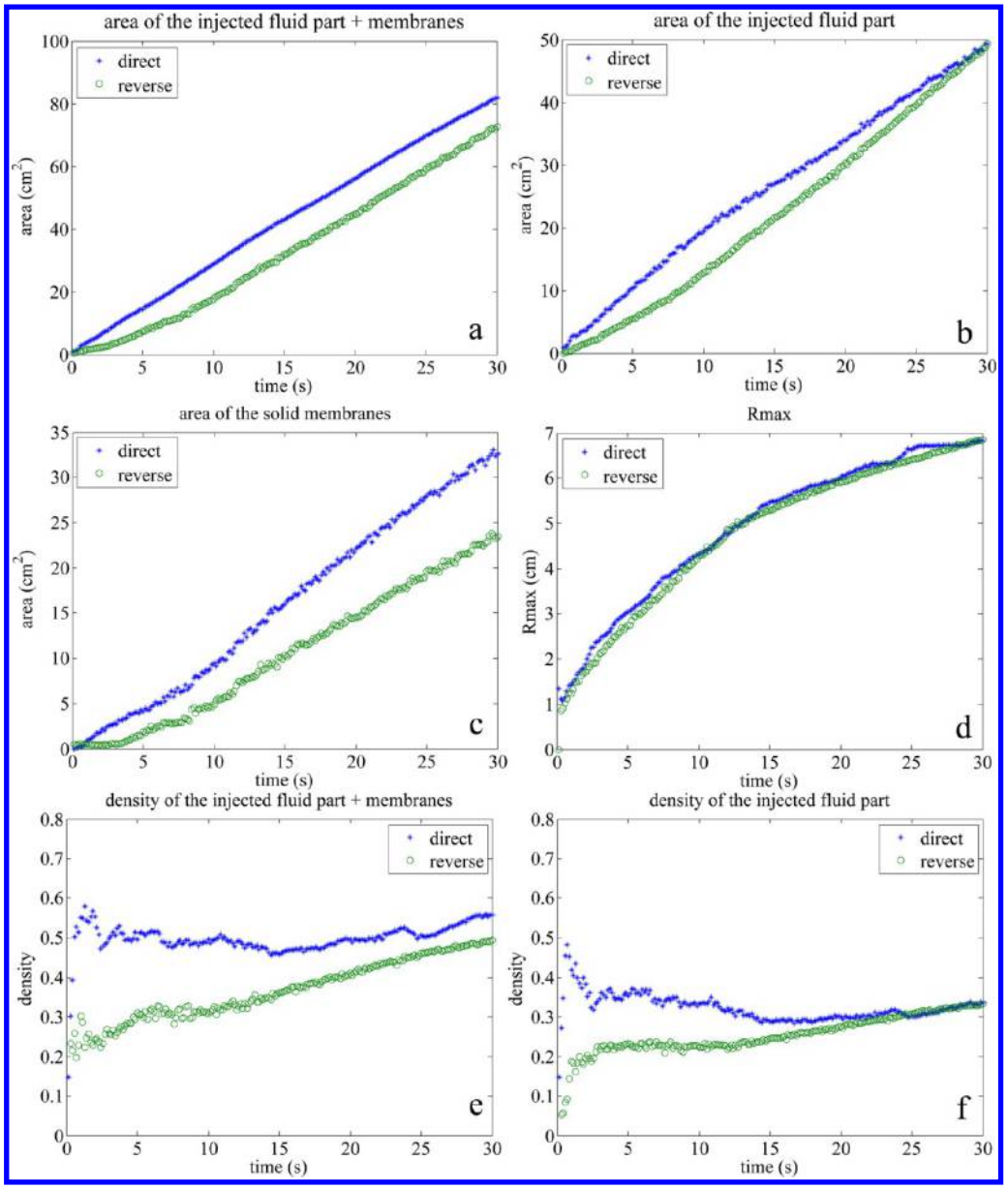

Figure 6. Evolution with time up to $t = 30$ s of (a) the area of the injected fluid + precipitate, (b) the area of the injected fluid part only, (c) the area of the precipitate layers only, (d) R_{max}, (e) the density constructed with the area of the injected fluid + precipitate layers, and (f) the density constructed from the area of the injected fluid part for the patterns of Figure 5.

We can discriminate the precipitate layers and the injected fluid part (inside the precipitate layers) that have different colors (light fluid and dark precipitates). Different thresholds for selecting the pixels of the digitized images enable us to obtain different areas. Even if there is always an error associated with the area determinations due to the presence of the injector and of the choice of an arbitrary threshold, we see in Figure 5b that a larger threshold captures both the precipitated parts and the injected fluid whereas for a lower threshold, only the solid parts are captured in Figure 5c. For the reverse case, in Figure 5e, only the fluid part is captured whereas in Figure 5f only the precipitate layers are shown. Depending on the four thresholds chosen, we are able to plot three different areas in Figure 6: the area of the injected fluid part, the area of the injected fluid + precipitate layers, and the area of the precipitate alone. Two different pattern densities are obtained from the fluid part only and from the fluid part + precipitate part.

Parts a−c of Figure 6 show comparable evolution for the different areas, even if the area of the direct case seems a bit larger. In Figure 6d, we can see that the direct and reverse experiments present the same R_{max} evolution with time, suggesting that the spirals of Figure 5 grow radially at the same speed. Finally, the two pattern densities (Figure 6e and Figure 6f) converge to very similar values (0.5−0.6 for the fluid + precipitate and 0.35 for the injected fluid part). A value of pattern density around 0.5 corresponds to an intermediate compact pattern between flowers and filaments.

Figures 7 and 8 show an intermediate concentration case with channels of spirals in both the direct and the reverse cases. One can see that for the direct case, R_{max} keeps a constant value after $t \approx 13$ s, once the spirals have reached a maximal distance from injection and further growth comes back in the interior of the circle. The growth of R_{max} is somewhat slower in the reverse case,

DOI: 10.1021/acs.jpcc.5b00599
J. Phys. Chem. C 2015, 119, 15067−15076

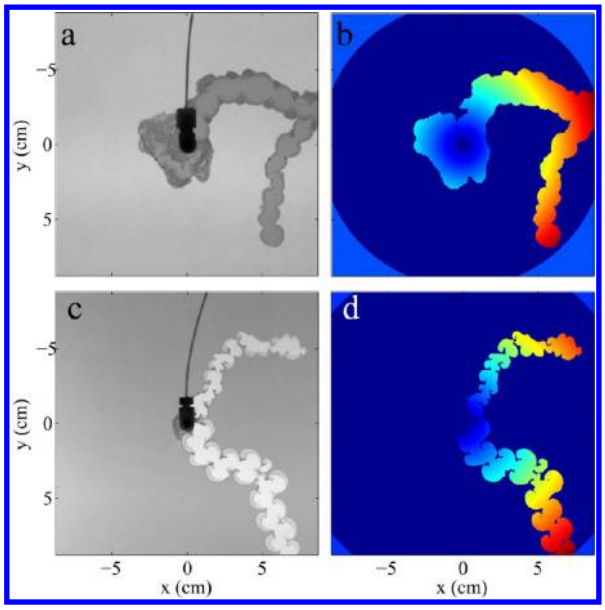

Figure 7. First line: direct case and second line: reverse case for C_{Co} = 0.63 M and C_{Si} = 1.25 M: (a, c) blue channel of the experimental snapshots; (b, d) $I \times r$ in false colors, with I the binarized picture and r the radial distance from the injection point. The dark blue disk enables us to visualize R_{max}. The field of view is 17.5 cm × 17.5 cm, and the picture is taken 30 s after the beginning of the injection.

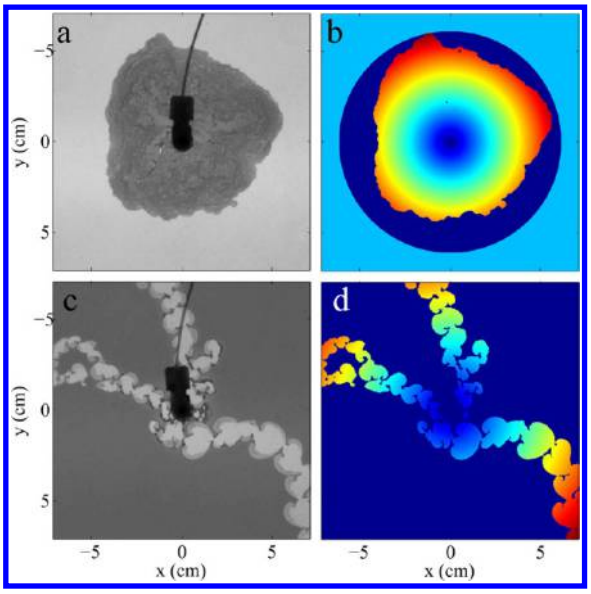

Figure 9. First line: direct case and second line: reverse case for C_{Co} = 1.25 M and C_{Si} = 1.25 M: (a, c) blue channel of the experimental snapshots; (b, d) $I \times r$ in false colors, with I the binarized picture and r the radial distance from the injection point. The dark blue disk enables us to visualize R_{max}. The field of view is 14.2 cm × 14.2 cm, and the picture is taken 30 s after the beginning of the injection.

but because the area of the direct case is somewhat larger, the densities are quite close.

Let us now examine a situation for which the direct and reverse cases are not similar at all. For example for C_{Co} = 1.38 M and C_{Si} = 1.25 M, the compact circular pink solid phase observed in the direct case is different from the reverse pattern made of a succession of spirals growing in channels. A similar case is analyzed in Figures 9 and 10 for 1.25 M for both concentrations. Both areas evolve quasi-linearly with a difference for the reverse case starting from the time $t \approx 19$ s when the structure reaches the border of the analysis window. We can clearly see that the R_{max} and pattern density evolutions in time are different. The channel of reverse spirals is growing faster in a given direction, whereas the direct compact pattern is growing more slowly, reaching a higher pattern density after 30 s (0.6 in the direct case and close to 0.1 for the reverse case). With these simple plots of the geometrical features of the global patterns it is possible to gain information on the growth properties and on the difference when reversing the injected and displaced reactants.

V. CONCLUSIONS

We have shown that in quasi-two-dimensional geometries, chemical gardens formed upon injection of a metallic salt into a silicate solution produce in general different patterns than in the reverse injection procedure. The differences have been discussed in terms of the relative influence of viscous or buoyancy-driven hydrodynamic instabilities when one of the two solutions is much more concentrated than the other. Another effect that is important is the amount of precipitate formed, which changes the cohesivity of the solid material and varies with the reactant concentrations while the pH does not seem to have a drastic influence. We have also computed the evolution in time of the precipitate pattern's area and density to confirm quantitatively that the properties of direct and reverse confined gardens can be quite different in some concentration regimes. In future work, more detailed investigation of the interplay between the hydrodynamic, chemical, and mechanical processes should be performed as a function of flow rate and more statistics should be performed to extract the essence of the growth of each pattern category. This should allow us to discriminate the relative

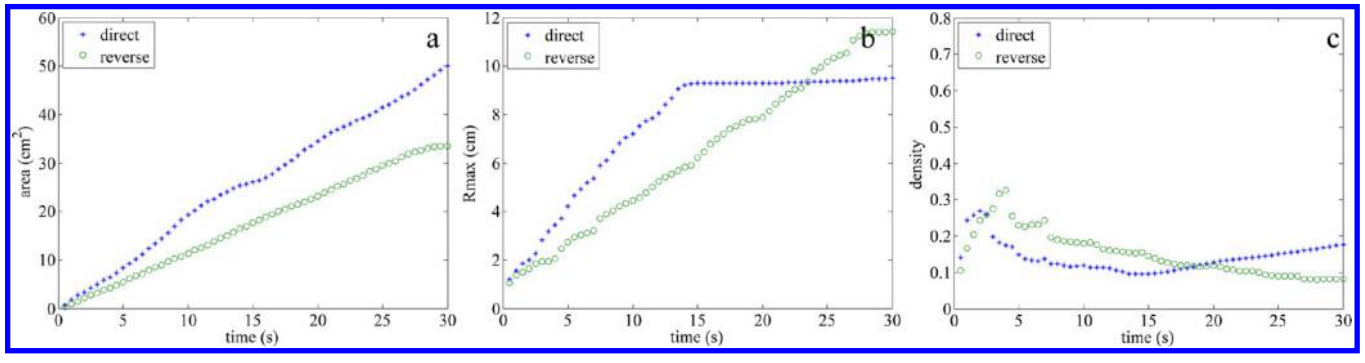

Figure 8. Evolution with time up to t = 30 s of (a) the area of the injected fluid + precipitate layers, (b) R_{max}, and (c) the pattern density constructed with the area of the injected fluid + precipitate layers for the patterns of Figure 7.

DOI: 10.1021/acs.jpcc.5b00599
J. Phys. Chem. C 2015, 119, 15067−15076

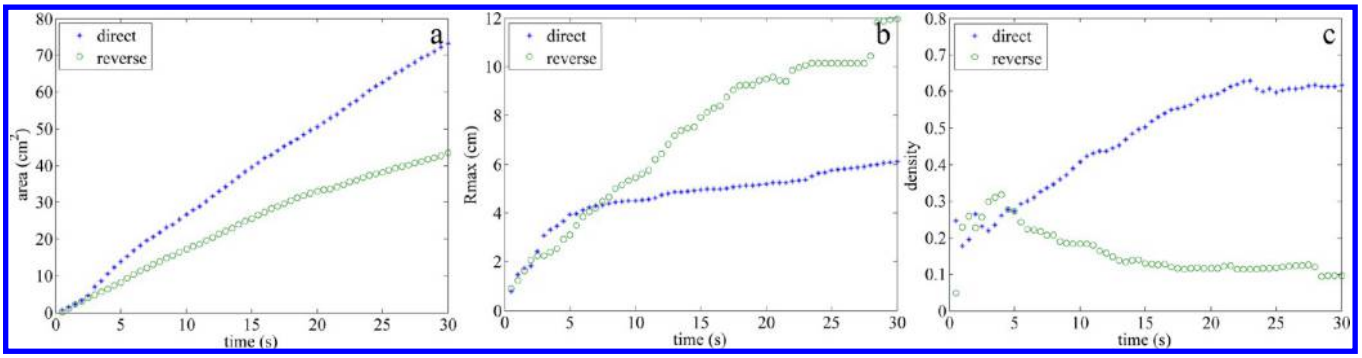

Figure 10. Evolution with time up to $t = 30$ s of (a) the area of the injected fluid + precipitate layers, (b) R_{max}, and (c) the pattern density constructed with the area of the injected fluid + precipitate layers for the patterns of Figure 9.

importance of the various chemical and physical processes at their origin, which is of major importance in nonlinear pattern formation and materials science, to name just two relevant fields.

AUTHOR INFORMATION

Notes

The authors declare no competing financial interest.

ACKNOWLEDGMENTS

We thank F. Brau for fruitful discussions. A.D. and F.H. thank PRODEX for financial support. A.D. acknowledges support from the FORECAST FRS-FNRS project. J.H.E.C. acknowledges the financial support of MICINN Grant FIS2013-48444-C2-2-P.

REFERENCES

(1) Saffman, P. G.; Taylor, G. I. The penetration of a fluid into a porous medium or Hele-Shaw cell containing a more viscous liquid. *Proc. R. Soc. London, Ser. A* **1958**, *245*, 312−329.
(2) Homsy, G. M. Viscous fingering in porous media. *Annu. Rev. Fluid Mech.* **1987**, *19*, 271−311.
(3) Chadam, J.; Ortoleva, P. Morphological instabilities in physico-chemical systems. *Earth-Sci. Rev.* **1990**, *29*, 175−181.
(4) Szymzak, P.; Ladd, A. J. C. The initial stages of cave formation: Beyond the one-dimensional paradigm. *Earth Planet. Sci. Lett.* **2011**, *301*, 424−432.
(5) Podgorski, T.; Sostarecz, M. C.; Zorman, S.; Belmonte, A. Fingering instabilities of a reactive micellar interface. *Phys. Rev. E* **2007**, *76*, 016202.
(6) Hejazi, S. H.; Trevelyan, P. M. J.; Azaiez, J.; De Wit, A. Viscous fingering of a miscible reactive A+B→C interface: a linear stability analysis. *J. Fluid Mech.* **2010**, *652*, 501−528.
(7) Gérard, T.; De Wit, A. Miscible viscous fingering induced by a simple A+B→C chemical reaction. *Phys. Rev. E* **2009**, *79*, 016308.
(8) Riolfo, L. A.; Nagatsu, Y.; Iwata, S.; Maes, R.; Trevelyan, P. M. J.; De Wit, A. Experimental evidence of reaction-driven miscible viscous fingering. *Phys. Rev. E* **2012**, *85*, 015304(R).
(9) Nagatsu, Y.; De Wit, A. Viscous fingering of a miscible reactive A +B→C interface for an infinitely fast chemical reaction: Nonlinear simulations. *Phys. Fluids* **2011**, *23*, 043103.
(10) Nagatsu, Y.; Ishii, Y.; Tada, Y.; De Wit, A. Hydrodynamic fingering instability induced by a precipitation reaction. *Phys. Rev. Lett.* **2014**, *113*, 024502.
(11) Glauber, J. R. *Furni Novi Philosophici*; Fabel: Amsterdam, 1646.
(12) Coatman, R. D.; Thomas, N. L.; Double, D. D. Studies of the growth of "silicate gardens" and related phenomena. *J. Mater. Sci.* **1980**, *15*, 2017−2026.
(13) Jones, D. E. H.; Walter, U. The silicate garden reaction in microgravity: a fluid interfacial instability. *J. Colloid Interface Sci.* **1998**, *203*, 286−293.
(14) Cartwright, J. H. E.; Garcia-Ruiz, J. M.; Novella, M. L.; Otalora, F. Formation of chemical gardens. *J. Colloid Interface Sci.* **2002**, *256*, 351−359.
(15) Tóth, A.; Horváth, D.; Smith, R.; McMahan, J. R.; Maselko, J. Phase diagram of precipitation morphologies in the Cu^{2+}-PO_4^{3-} System. *J. Phys. Chem. C* **2007**, *111*, 14762−14767.
(16) Maselko, J.; Borisova, P.; Carnahan, M.; Dreyer, E.; Devon, R.; Schmoll, M.; Douthat, D. Spontaneous formation of chemical motors in simple inorganic systems. *J. Mater. Sci. Lett.* **2005**, *40*, 4671−4673.
(17) Pantaleone, J.; Tóth, A.; Horváth, D.; Rother McMahan, J.; Smith, R.; Butki, D.; Braden, J.; Mathews, E.; Geri, H.; Maselko, J. Oscillations in a chemical garden. *Phys. Rev. E* **2008**, *77*, 046207.
(18) Pantaleone, J.; Tóth, A.; Horváth, D.; RoseFigura, L.; Morgan, W.; Maselko, J. Pressure oscillations in a chemical garden. *Phys. Rev. E* **2009**, *79*, 056221.
(19) Cooper, G. J. T.; Boulay, A. G.; Kitson, P. J.; Ritchie, C.; Richmond, C. J.; Thiel, J.; Gabb, D.; Eadie, R.; Long, D.-L.; Cronin, L. Osmotically driven crystal morphogenesis: a general approach to the fabrication of micrometer-scale tubular architectures based on polyoxometalate. *J. Am. Chem. Soc.* **2011**, *133*, 5947−5954.
(20) Cooper, G. J. T.; Bowman, R. W.; Magennis, R. W.; Fernandez-Trillo, F.; Alexander, C.; Padgett, M. J.; Cronin, L. Directed assembly of inorganic polyoxometalate-based micrometer-scale tubular architectures by using optical control. *Angew. Chem., Int. Ed.* **2012**, *51*, 12754−12758.
(21) Pagano, J. J.; Bánsági, T., Jr.; Steinbock, O. Bubble-templated and flow-controlled synthesis of macroscopic silica tubes supporting zinc oxide nanostructures. *Angew. Chem., Int. Ed.* **2008**, *47*, 9900−9903.
(22) Barge, L. M.; Doloboff, I. J.; Russell, M. J.; VanderVelde, D.; White, L. M.; Stucky, G. D.; Baum, M. M.; Zeytounian, J.; Kidd, R.; Kanik, I. Pyrophosphate synthesis in iron mineral films and membranes simulating prebiotic submarine hydrothermal precipitates. *Geochim. Cosmochim. Acta* **2014**, *128*, 1−12.
(23) Makki, R.; Al-Humiari, M.; Dutta, S.; Steinbock, O. Hollow microtubes and shells from reactant-loaded polymer beads. *Angew. Chem., Int. Ed.* **2009**, *48*, 8752−8756.
(24) Makki, R.; Roszol, L.; Pagano, J. J.; Steinbock, O. Tubular precipitation structures: materials synthesis under non-equilibrium conditions. *Philos. Trans. R. Soc. A* **2012**, *370*, 2848−2865.
(25) Makki, R.; Steinbock, O. Nonequilibrium synthesis of silica-supported magnetite tubes and mechanical control of their magnetic properties. *J. Am. Chem. Soc.* **2012**, *134*, 15519−15527.
(26) Roszol, L.; Makki, R.; Steinbock, O. Postsynthetic processing of copper hydroxide-silica tubes. *Chem. Commun.* **2013**, *49*, 5736−5738.
(27) Makki, R.; Ji, X.; Mattoussi, H.; Steinbock, O. Self-organized tubular structures as platforms for quantum dots. *J. Am. Chem. Soc.* **2014**, *136*, 6463−6469.
(28) Russell, M. J.; Hall, A. The emergence of life from iron monosulphide bubbles at a submarine hydrothermal redox and pH front. *J. Geol. Soc.* **1997**, *154*, 377−402.

DOI: 10.1021/acs.jpcc.5b00599
J. Phys. Chem. C 2015, 119, 15067−15076

(29) Barge, L. M.; Doloboff, I. J.; White, L. M.; Stucky, G. D.; Russell, M. J.; Kanik, I. Characterization of iron-phosphate-silicate chemical garden structures. *Langmuir* **2012**, *28*, 3714−3721.
(30) Thouvenel-Romans, S.; Steinbock, O. Oscillatory growth of silica tubes in chemical gardens. *J. Am. Chem. Soc.* **2003**, *125*, 4338−4341.
(31) Pagano, J. J.; Bánsági, T., Jr.; Steinbock, O. Tube formation in reverse silica gardens. *J. Phys. Chem. C* **2007**, *111*, 9324−9329.
(32) Haudin, F.; Cartwright, J. H. E.; Brau, F.; De Wit, A. Spiral precipitation in confined chemical gardens. *Proc. Natl. Acad. Sci. U.S.A.* **2014**, *111*, 17363−17367.
(33) Haudin, F.; Brasiliense, V.; Cartwright, J. H. E.; Brau, F.; De Wit, A. Genericity of confined chemical garden patterns with regard to changes in the reactants. *Phys. Chem. Chem. Phys.* **2015**, *17*, 12804−12811.
(34) Bohner, B.; Schuszter, G.; Berkesi, O.; Horváth, D.; Tóth, A. Self-organization of calcium oxalate by flow-driven precipitation. *Chem. Commun.* **2014**, *50*, 4289−4291.
(35) Pagano, J. J.; Thouvenel-Romans, S.; Steinbock, O. Compositional analysis of copper-silica precipitation tubes. *Phys. Chem. Chem. Phys.* **2007**, *9*, 110−116.
(36) Cartwright, J. H. E.; Escribano, B.; Sainz-Diaz, C. I. Chemical-garden formation, morphology, and composition. I. Effect of the nature of the cations. *Langmuir* **2011**, *27*, 3286−3293.
(37) Haudin, F.; Riolfo, L. A.; Knaepen, B.; Homsy, G. M.; De Wit, A. Experimental study of a buoyancy-driven instability of a miscible horizontal displacement in a Hele-Shaw cell. *Phys. Fluids* **2014**, *26*, 044102.
(38) Baker, A.; Tóth, A.; Walkush, J.; Ali, A. S.; Morgan, W.; Kukovecz, A.; Pantaleone, J. J.; Maselko, J. Precipitation pattern formation in the copper(II) oxalate system with gravity flow and axial symmetry. *J. Phys. Chem. A* **2009**, *113*, 8243−8248.
(39) Nagatsu, Y.; Matsuda, K.; Kato, Y.; Tada, Y. Experimental study on miscible viscous fingering involving viscosity changes induced by variations in chemical species concentrations due to chemical reactions. *J. Fluid Mech.* **2007**, *571*, 475−493.

DOI: 10.1021/acs.jpcc.5b00599
J. Phys. Chem. C 2015, 119, 15067−15076